

Event selection and kinematic calculations in DØ Higgs analysis

Brian Allgeier
Department of Physics and Astronomy
University of Kentucky
Lexington, Kentucky

Particle Physics Division
Fermi National Accelerator Laboratory
Batavia, Illinois

August 5, 2014

Abstract

Standard Model Higgs predictions have been studied over the past several years at the DØ detector at Fermilab. A brief introduction to the Standard Model and the Higgs boson is given, as well as a briefer insight to the workings of the Tevatron accelerator and the DØ detector. An overview of past analyses using multivariate methods is given with current results. In order to better visualize and understand the phenomena within the detector, many promising Higgs event displays are created and explained. The author also attempts kinematic calculations in order to gain a deeper understanding of the Higgs events, with particular emphasis on the dijet angle between the decay products of the Higgs boson. It is concluded that many variables of the event, such as this angle, can be successfully understood via simple kinematic calculations, although one must account for the wide range of total energy among possible events due to the nature of parton energies determined by parton distribution functions.

1 Introduction to the theory

A. Standard Model The Standard Model is particle physics’ most complete theory thus far, giving extremely accurate predictions for vast amounts of physical phenomena within the universe. Although this model does not incorporate everything we observe, it does a very substantial job in the realm of particle physics. Of the four fundamental forces known, the Standard Model gives very precise theoretical explanations for three: the strong nuclear force, electromagnetism, and the weak nuclear force. The organization of all known particles described by the Standard Model is beautifully displayed in a table such as Figure 1, much like all known atoms are displayed within the Periodic Table of Elements.


















mass →	$\approx 2.3 \text{ MeV}/c^2$	$\approx 1.275 \text{ GeV}/c^2$	$\approx 173.07 \text{ GeV}/c^2$	0	$\approx 126 \text{ GeV}/c^2$
charge →	$2/3$	$2/3$	$2/3$	0	0
spin →	$1/2$	$1/2$	$1/2$	1	0
					
	up	charm	top	gluon	Higgs boson
	$\approx 4.8 \text{ MeV}/c^2$	$\approx 95 \text{ MeV}/c^2$	$\approx 4.18 \text{ GeV}/c^2$	0	
	$-1/3$	$-1/3$	$-1/3$	0	
	$1/2$	$1/2$	$1/2$	1	
					
	down	strange	bottom	photon	
	$0.511 \text{ MeV}/c^2$	$105.7 \text{ MeV}/c^2$	$1.777 \text{ GeV}/c^2$	$91.2 \text{ GeV}/c^2$	
	-1	-1	-1	0	
	$1/2$	$1/2$	$1/2$	1	
					
	electron	muon	tau	Z boson	
	$< 2.2 \text{ eV}/c^2$	$< 0.17 \text{ MeV}/c^2$	$< 15.5 \text{ MeV}/c^2$	$80.4 \text{ GeV}/c^2$	
	0	0	0	± 1	
	$1/2$	$1/2$	$1/2$	1	
					
	electron neutrino	muon neutrino	tau neutrino	W boson	

Figure 1: Table of elementary particles described by the Standard Model. Matter consists of fermions such as quarks (violet) and leptons (green). Forces are carried by bosons (red). The Higgs boson (yellow) allows for many particles to be massive through the Higgs mechanism.

The fundamental forces are the means by which matter interacts with other matter. The Standard Model explains that matter is comprised of leptons and quarks, which are all spin- $\frac{1}{2}$ particles. (These kinds of particles are called fermions, because they obey Fermi-Dirac statistics.) Electrons (e), muons (μ), and neutrinos (ν) are all examples of leptons, as well as their antiparticles (for example, the positron, e^+). There are many flavors of quarks as well, such as the up (u) and down (d) quarks, which form the nucleons (protons and neutrons, p and n) within the nuclei of atoms.

These forms of matter interact via gauge bosons, which are often known as the force-carriers of their respective interactions. (These particles carry integral spin, and follow Bose-Einstein statistics.) For example, particles which interact electromagnetically do so via the exchange of photons (γ); meanwhile quarks, which interact through the strong force (and also electromagnetically), exchange gluons (g), the carrier of the strong nuclear force. The electromagnetic force is the source of chemistry and molecular structure, which is essentially the study of electron exchange between atoms. The strong force explains changes on a nuclear level, such as fusion and fission.

The weak force is not nearly as strong as electromagnetism or the strong nuclear force. However, it is still the primary source of radioactive decay of unstable particles. The force carriers of the weak force are the W and Z bosons. Unlike the photon or gluon, interestingly, the weak bosons have non-zero mass. However, it was discovered that at sufficiently high energies, this mass seems to disappear to zero; this occurs within the energy realm where the weak force becomes united with electromagnetism, theoretically described by the electroweak theory. At lower energies, this symmetry between the two forces is broken, and they are separated into the two distinct phenomena we observe today. This peculiarity of symmetry-breaking seems to be deeply related to the Higgs mechanism and to the Higgs boson itself.

B. Higgs boson The Higgs Boson seems to be quite a necessary extension to the Standard Model in order to accurately explain nature as we see her today. Without the Higgs, all the particles of the Standard Model would necessarily be massless. Obviously, this is not what is observed for the vast majority of particles in the universe. In order to counteract this inaccuracy of the model, the Higgs field was introduced.

At the critical temperature when the electroweak symmetry breaks, three of the four components of the Higgs field are lost to the individuality of the weak bosons. In this process, the observed masses of the weak bosons naturally fall out of the theory as a mathematical consequence. The single component of the Higgs field which remains afterward at lower temperatures becomes the Higgs particle. The Higgs mechanism explains not only the masses of the weak bosons, but it also seems to possibly explain the mass of the other massive particles (leptons and quarks) as well.

Theoretically, it should be possible to observe the Higgs particle indirectly, at least for a fleeting moment, at very large temperatures. This is currently possible at Fermilab due to the joint effort of high-energy colliders, such as the Tevatron, and particle detectors such as DØ. The goal of these experiments is not only to find substantial evidence of the Higgs, but to also identify the mass of the new particle, because this value is not predicted by the Standard Model. In 2012, the Large Hadron Collider at CERN announced discovery of a new particle which seems to fit the Higgs' profile. This new particle was identified to have a mass of approximately 125 GeV, and is now commonly believed to be the Higgs boson.

2 Methods of experimentation

A. The Tevatron At about 1 km in radius, the Tevatron was the largest particle accelerator in the world at its completion in 1983, located at Fermi National Accelerator Laboratory (Fermilab) in Batavia, Illinois (although it is currently superseded by CERN's Large Hadron Collider in Geneva, Switzerland). Its name is derived from the ability to accelerate protons and antiprotons to very nearly 1 TeV of energy each. The Tevatron is a collider machine; therefore, separate proton and antiproton beams are accelerated to that peak energy each and then collided at the sight of a detector, which measures the aftermath of the collision. Due to the colliding design, the Tevatron is able to reach center-of-mass energies of about 1.96 TeV. The purpose of these high-energy collisions is to recreate the environment of the universe shortly after the Big Bang. These great energies allow for the study of new physics, such as the Higgs boson.

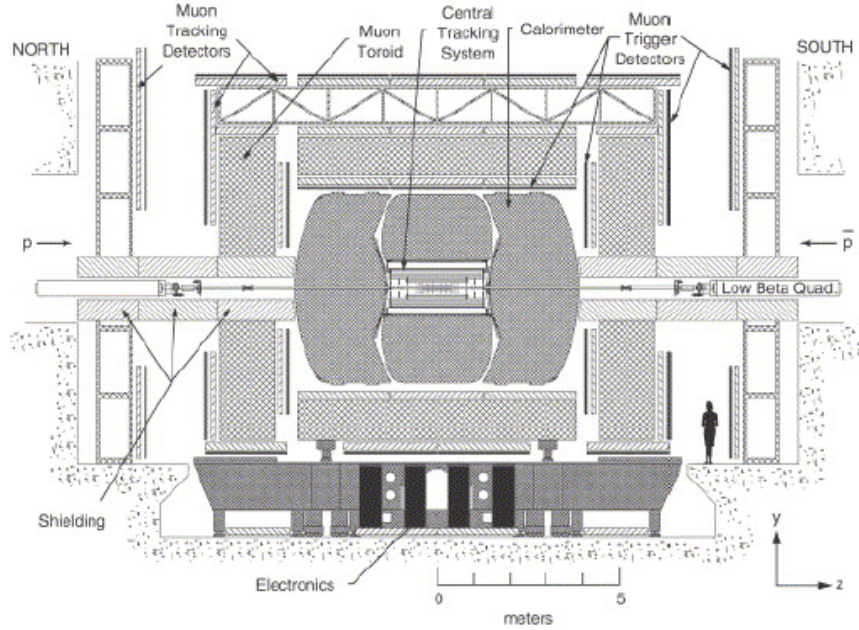


Figure 2: The upgraded DØ Detector at Fermilab, comprised of many layers, including (from innermost outward) particle tracking system, calorimeter, and muon detection system.²

B. The DØ detector In order to closely study such energetic phenomena, a detector is needed in addition to the accelerator. The data analyzed in this paper was gathered during Run II of the DØ detector. Particle detectors are made of many layers of extremely complicated detection equipment (a simplification of which is shown in Figure 2) in order to measure the properties of newly created particles as accurately and consistently as possible.

The innermost layer of DØ (closest radially to the beamline and interaction point) is the particle tracking system. Silicon sensors within the silicon microstrip tracker are responsible for the trajectory tracking of a large amount of the innermost particles. Outside of this layer is the central fiber tracker composed of scintillating fibers, which are responsible for light production as charged particles pass through, giving readable detection signals. The calorimeter is the next layer of the detector; as particles pass through layers of uranium, they decay and spray into a shower of particles. These newly created, lower energy particles are then able to be detected by leaving traces of ionization within a section of liquid argon, allowing for precise measurements of the original particles' energies. The majority of particles produced by a collision will have been stopped at this point in the detector. However, muons tend to pass through these layers without leaving much of a trace; therefore, an outer muon detection system exists on DØ in order to measure the trajectories and energies of these particles before they escape. Neutrinos, however, are extremely difficult to be detected with this instrumentation (or any sort of instrumentation at all), and are therefore accounted for as undetected, missing energy.

When taking data, massive numbers of events (several million) occur within the detector every second. Not all of this event information can be gathered and stored at such high rates, so a triggering system filters out all uninteresting events while keeping all interesting events, such as possible Higgs-like events (including actual signal as well as background events). Although the majority of events within the detector are not kept for analysis, there still remains massive amounts of data to be analyzed.

3 Event selection

A. Event overview The primary goal in the analysis of this experimental data is to discriminate any background data from the Higgs signal. Because a Higgs event occurs so rarely compared to other events, this separation process takes much time and effort. Higgs events may occur in several ways, each of which with its own probability of occurring and its own ease of recognition. At DØ the $WH \rightarrow l\nu b\bar{b}$ channel is the most promising and productive channel for Higgs analysis. The representative Feynman diagram is shown in Figure 3.

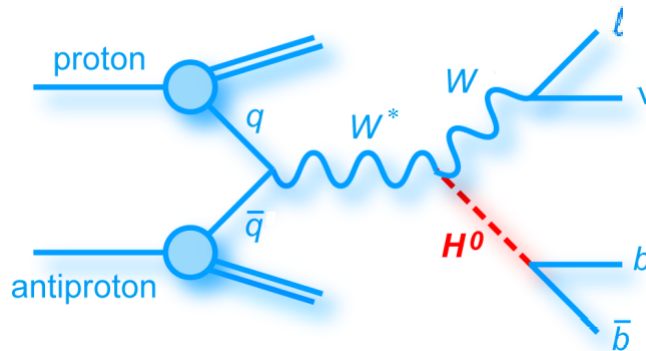


Figure 3: Feynman diagram of Higgs event $WH \rightarrow l\nu b\bar{b}$, referred to as the WH channel.²

In this channel, a (virtual) W^* boson (created by quark-antiquark interaction) radiates a Higgs particle. The (real) W boson then decays into a lepton-neutrino pair, and the Higgs proceeds to decay into a quark-antiquark pair. At the assumed Higgs mass of roughly 125 GeV, these quarks should most likely be of the bottom flavor. Other channels exist for Higgs production; however, these channels, such as those studied at CERN, are not practically possible due to the Tevatron's lower energies.

Each of the background channels produces a very similar final topology to the WH channel, as shown in Figure 4. Most notably, in many channels, a lepton is produced (either an electron or muon) together with a neutrino (which is unobserved). Also, parton jets are created, ideally by two bottom quarks in the WH channel. However, these jets are difficult to identify and may be confused with other signals or jets created by separate background events instead of a Higgs signal.

The method used to attempt to identify these parton jets is known as b-tagging. The geometry of the jets produced in an event is analyzed and placed into a certain category

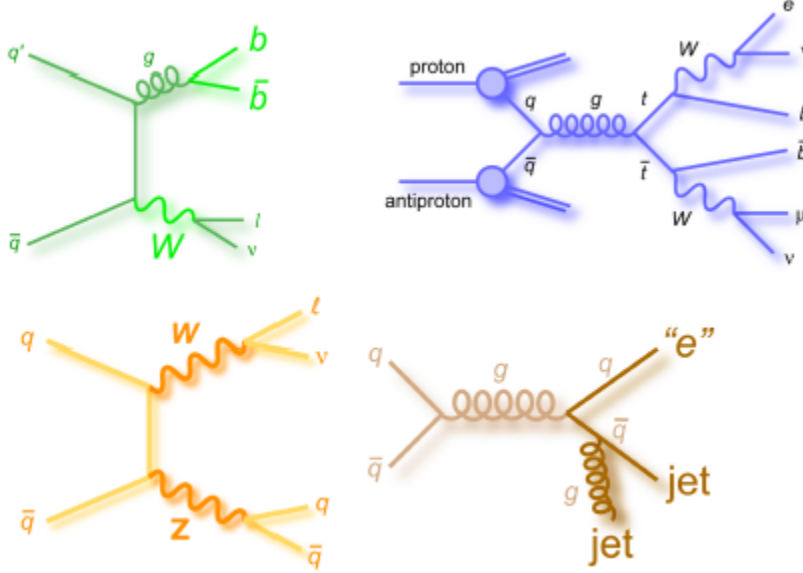


Figure 4: Feynman diagrams of a few possible background events which may occur at DØ, all of which have very similar final state topologies to an actual WH signal event.²

depending on the confidence of the correctness of the tagging. Events which display strong similarity with the geometry of actual bottom quark jets are placed into a "tight" tag bin. Those which display less similarity are placed in medium-tag or loose-tag bins and can be identified as bottom jets with less confidence. In order to maintain the most accuracy possible, all other events which do not contain two tight tags are often cut from the data.

The total number of expected events, both signal and background, are tabulated in Figures 5 and 6. Each event contains two parton jets and are separated into categories based on the b-tagging of the event. The two tables are also separated by the lepton produced (either electron or muon). It can easily be seen that signal events are expected in far fewer numbers than all other background events.

B. Multivariate methods In past analyses, a multivariate analysis (MVA) was used. This method uses computational structures in the ROOT library known as boosted decision trees (BDTs) to attempt to distinguish signal from background events. Multiple variable values are measured for each event, each of which may be able to distinguish signal from background events if studied carefully. These slightly discriminating variables are able to be analyzed together effectively as one variable able to discriminate more strongly than any one variable by itself. The BDTs, through many repeated trials, attempt to decide whether a certain event variable belongs to signal or background. In order to do this effectively with actual data, the BDTs must be "trained" on Monte Carlo simulations of certain events which are known to be either signal or background. Once applied to actual data, the MVA output is a number between -1 and 1 , known as the discriminant. This number is a reflection of how "Higgs-like" the event appears to be, or if it rather seems like a certain background instead.

	Pretag	1 tight <i>b</i> -tag	2 loose <i>b</i> -tags	2 med. <i>b</i> -tags	2 tight <i>b</i> -tags
$VH \rightarrow \ell \nu b \bar{b}$	19.2	6.1	1.6	2.3	3.9
$H \rightarrow VV \rightarrow \ell \nu j \bar{j}$	13.2	1.0	0.2	0.03	0
$VH \rightarrow VVV \rightarrow \ell \nu j \bar{j} j \bar{j}$	7.1	0.7	0.1	0.02	0.01
Diboson	2877	269	55.7	21.5	18.6
$V + (g, u, d, s)$ -jets	89728	3121	892	63.6	6.4
$V + (b \bar{b}/c \bar{c})$	13596	2595	480	338	343
top ($t \bar{t}$ + single top)	1932	703	137	184	252
Multijet	41986	2407	619	169	104
Total background expectation	150158	9103	2187	779	727
Total background uncertainty	7423	887	192	92	92
Observed events	150118	8946	2187	702	621

Figure 5: Table of expected signal and background events which produce an electron.²

	Pretag	1 tight <i>b</i> -tag	2 loose <i>b</i> -tags	2 med. <i>b</i> -tags	2 tight <i>b</i> -tags
$VH \rightarrow \ell \nu b \bar{b}$	17.4	5.0	1.4	2.1	3.5
$H \rightarrow VV \rightarrow \ell \nu j \bar{j}$	10.9	0.8	0.2	0.04	0
$VH \rightarrow VVV \rightarrow \ell \nu j \bar{j} j \bar{j}$	5.1	0.4	0.1	0.02	0
Diboson	2904	383	68.5	39.1	44.6
$V + (g, u, d, s)$ -jets	78109	2645	807	60.9	5.5
$V + (b \bar{b}/c \bar{c})$	13445	2531	486	341	335
top ($t \bar{t}$ + single top)	3448	688	126	156	202
Multijet	28486	1560	367	121	87.6
Total background expectation	126425	7813	1856	720	678
Total background uncertainty	7576	835	177	87	85
Observed events	126811	7460	1870	656	544

Figure 6: Table of expected signal and background events which produce a muon.²

In order for event to be considered as a possible signal event by the analysis framework, it must pass a series of selection cuts based on the values of certain variables that a Higgs event is likely to have. These cuts are currently the following (in units of GeV): lepton $P_T > 15$, jet $P_T > 20$, and missing $E_T > 15$ (for electron) or $E_T > 20$ (for muon). These conditions must be satisfied for an event to continue through the framework. A histogram of dijet mass for all two-tight-tagged events is shown in Figure 7. MVA plots against all major backgrounds are shown as well. As stated previously, the greater the MVA value, the "Higgsier" the event seems to be, as interpreted by the framework; the lower the MVA value is, the more likely it is to be a certain background event. The highest MVA-valued events are of most interest because these most likely correspond to the majority of the signal. The low MVA-valued events are most likely background; these events are to be removed via a series of selection cuts to isolate the signal as best as possible and to increase the signal-to-background ratio.

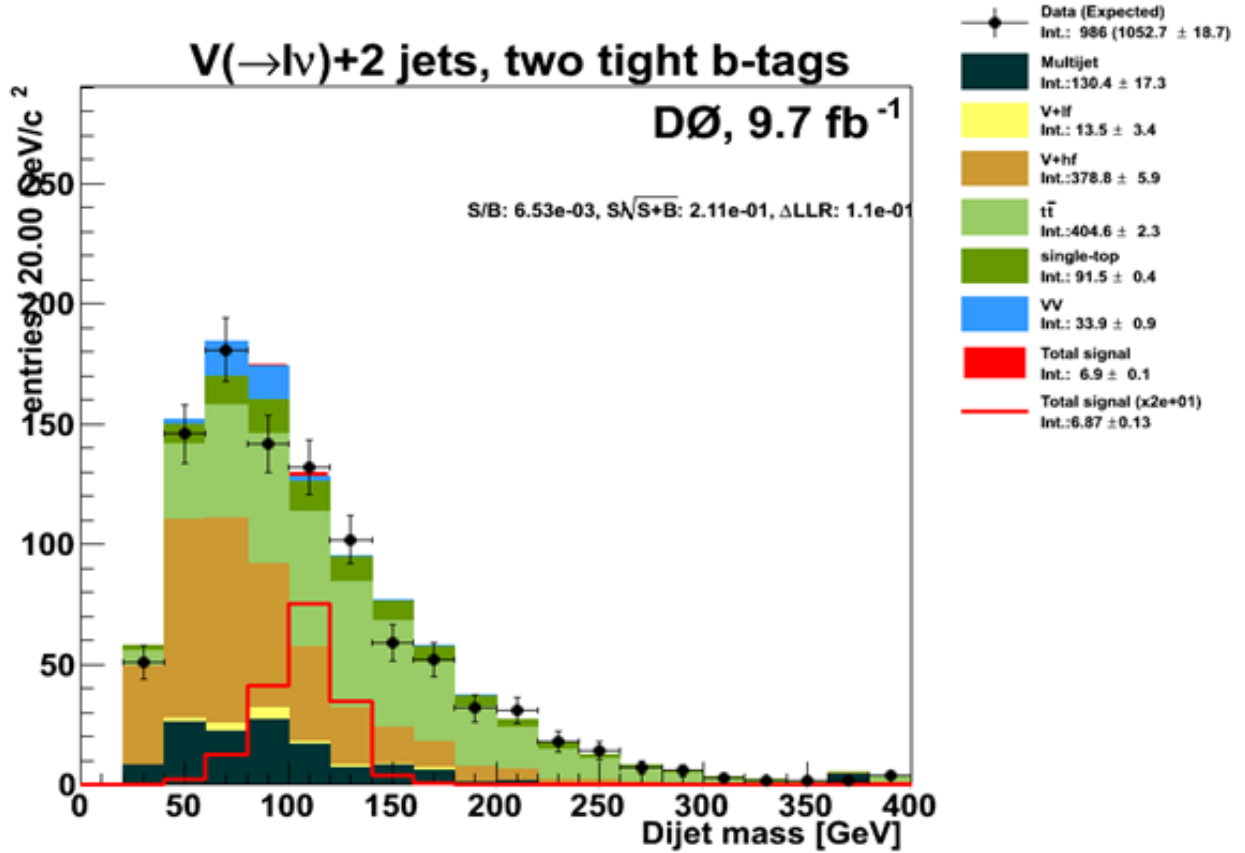


Figure 7: Histogram of the dijet mass within two-tight-tagged events before any MVA cuts are made to the data. The colored bins of the histogram represent Monte Carlo predictions of the background events. The red line is an amplification of the predicted WH signal because it is too small to be seen in comparison to the many backgrounds. Actual data is shown on the histogram as well (black points with error bars). If the data is accurately predicted by Monte Carlo simulation, the data points will lie precisely at the top of each event bin stack. [This histogram, and the following, is the product of the past efforts of the WH DØ group.]

The first MVA plot is Higgs vs. $t\bar{t}$ (Figure 8). A cut was made at $MVA_{t\bar{t}} > 0$ in order to eliminate a vast majority of the chosen background without much signal loss. This cut was very effective because the signal and background were very well-separated via MVA. The resulting dijet mass histogram is shown (Figure 9).

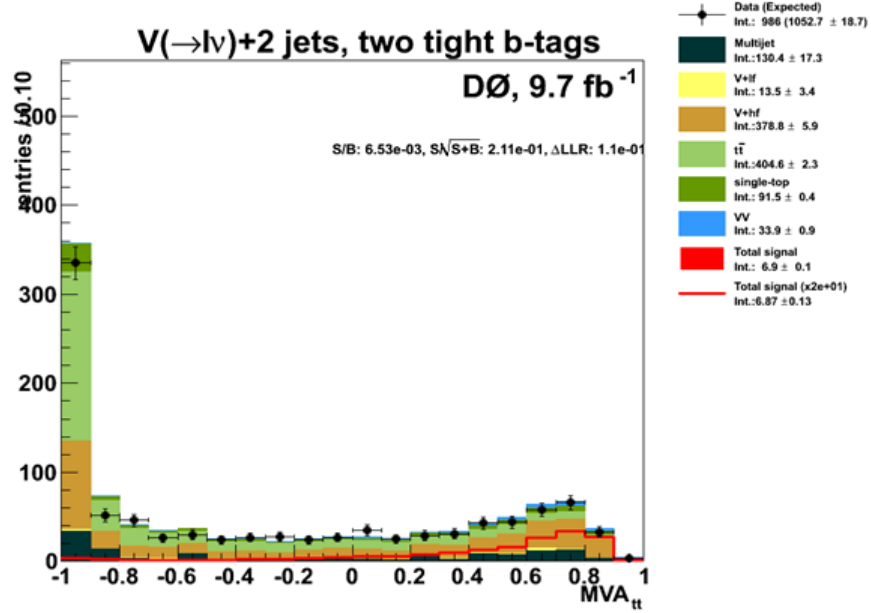


Figure 8: MVA plot, WH vs. $t\bar{t}$

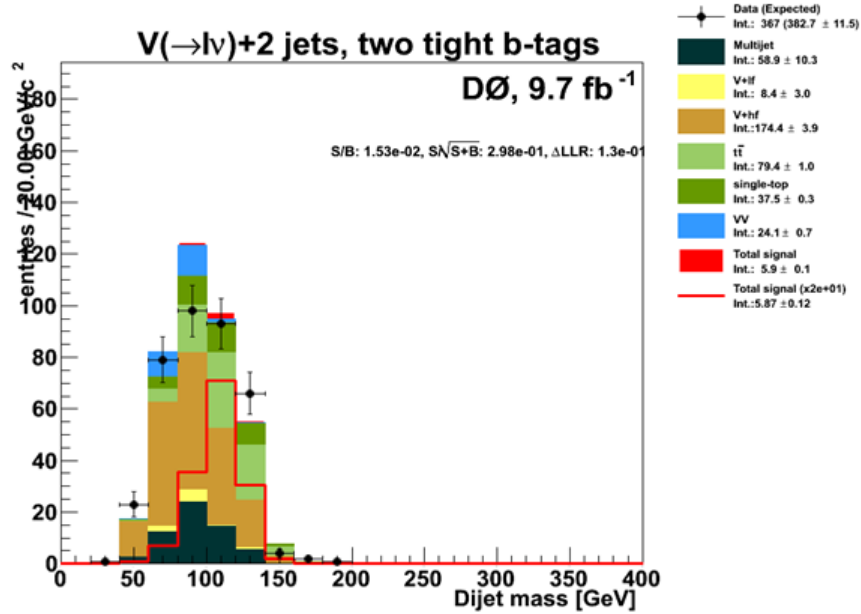


Figure 9: Dijet Mass, Post $t\bar{t}$ cut

An MVA plot for WH versus the vector boson plus jet background (VJ) is displayed (Figure 10). There is less discrimination within this MVA plot than in the last; nevertheless, another cut for $MVA_{VJ} > 0$ was performed. As can be seen in the dijet mass histogram (Figure 11), the data is quite centered around the expected Higgs' mass of 125 GeV.

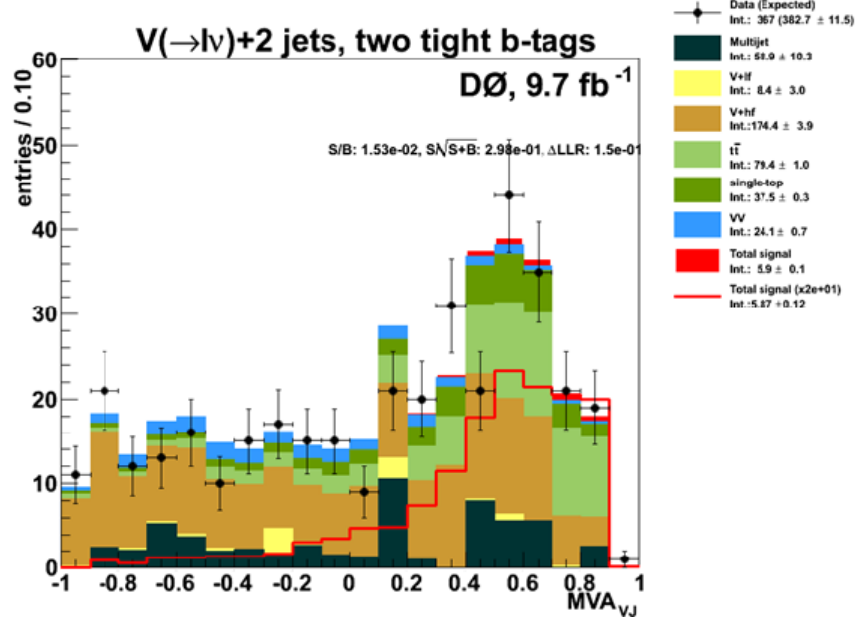


Figure 10: MVA plot, WH vs. VJ

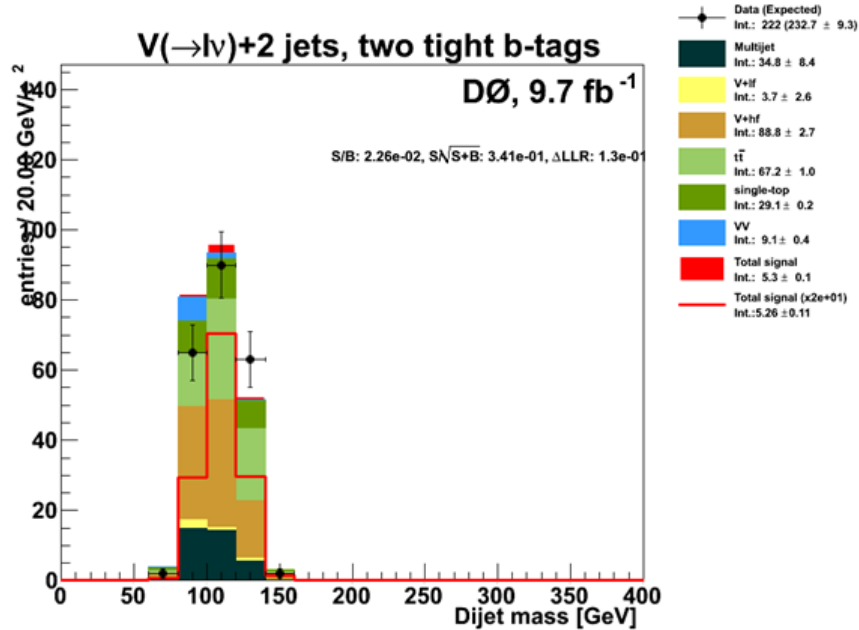


Figure 11: Dijet Mass, Post $t\bar{t} + VJ$ cuts

The next background to discriminate against is diboson (VV), as shown in the MVA plot (Figure 12). There is little effective discrimination in this case, but still another cut is made at $MVA_{VV} > 0$. In the subsequent mass histogram (Figure 13), the signal count is clearly visible at the top of the background stack.

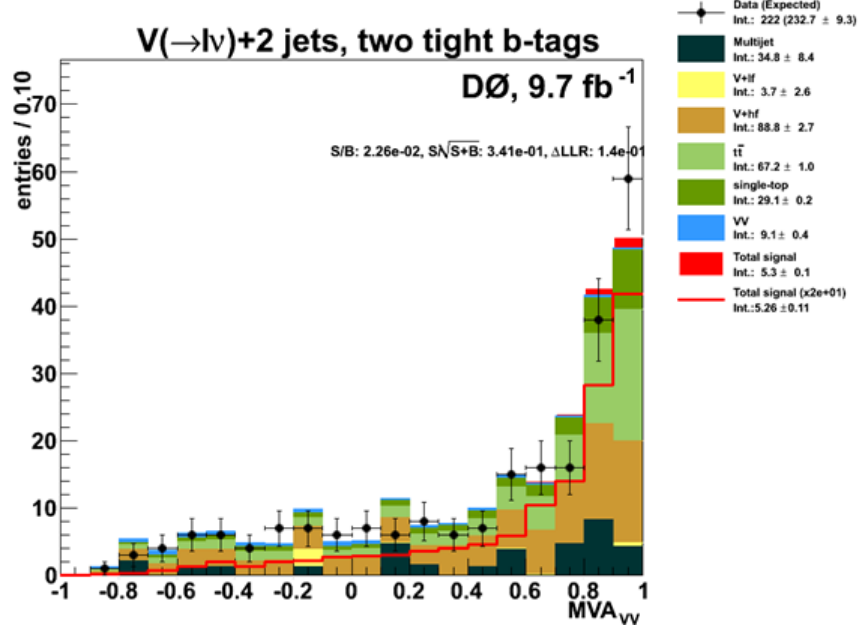


Figure 12: MVA plot, WH vs. VV

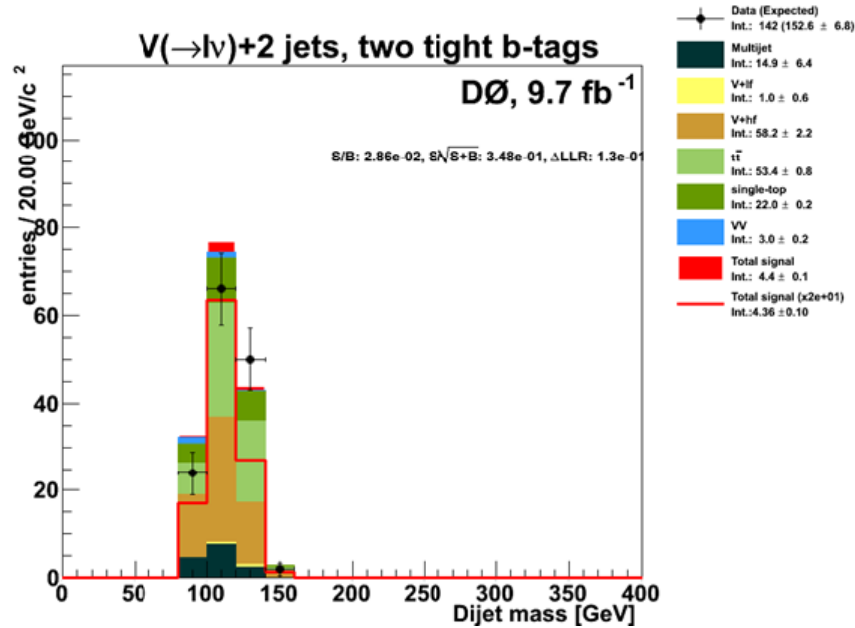


Figure 13: Dijet Mass, Post $t\bar{t} + VJ + VV$ cuts

The final cut is made against the multijet background (MJ) at $MVA_{MJ} > 0.4$, eliminating much of the chosen background count (Figure 14). After all four MVA cuts, the final dijet mass histogram is shown (Figure 15). The final signal-to-background ratio is roughly 3%, which was an increase by a factor of about 4.7 from the original S/B value.

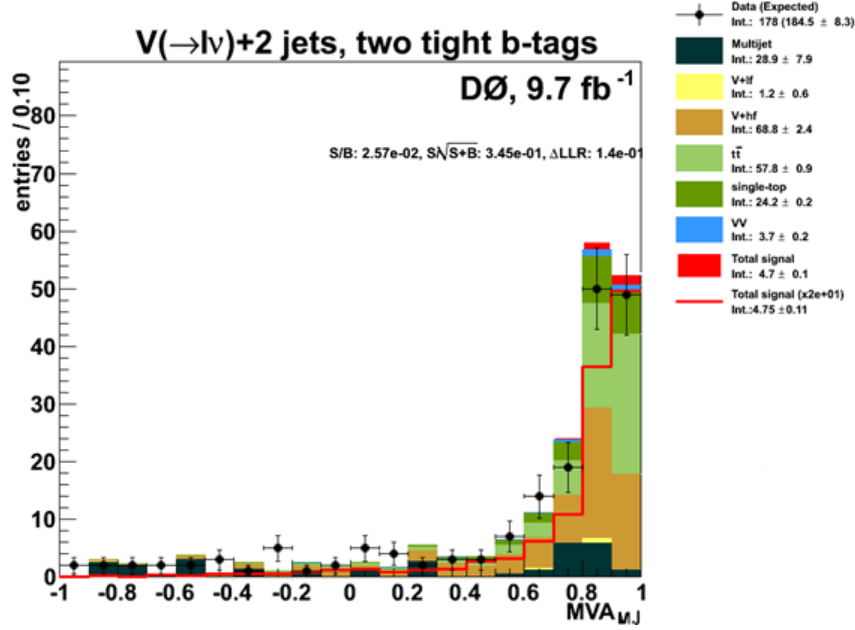


Figure 14: MVA plot, WH vs. MJ

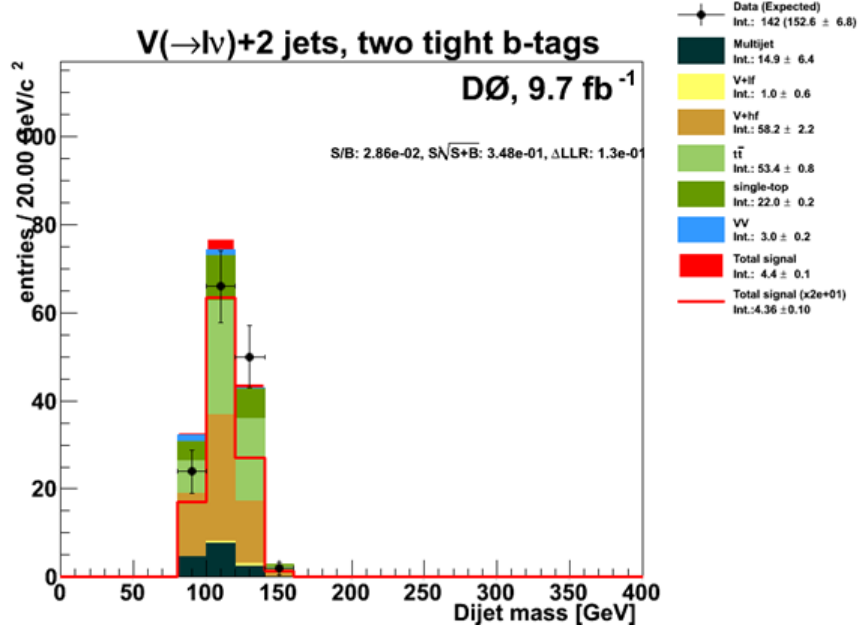


Figure 15: Dijet Mass, Post $t\bar{t} + VJ + VV + MJ$ cuts

C. Higgs event displays Using DØCAFVis software, realistic displays of high energy events within the detector are able to be virtually recreated. Events with the highest MVA values are selected to be displayed. The original event displays reveal great amounts of detailed information, much of which is unnecessary or distracting from more important factors. These displays must be edited slightly in order to be as useful as possible. For example, most particle tracks identified by the detector are unimportant in understanding the nature of the event, and should be removed in order to decrease the clutter within the image, as well as many small calorimeter hits. Low-energy jets which are most likely resolved by mistake are removed as well, often leaving the two highest energy jets (the two "leading jets"). Ideally, these two jets correspond to the $b\bar{b}$ decay products of the Higgs in a WH event. Labels are created for the four most important factors in any WH event: the two leading jets, the lepton track, and the missing transverse energy. The event display of a likely Higgs event is shown in Figure 16. It is important to note that the two leading jets are pointing away from the lepton-neutrino pair; these two systems represent the decays of the original Higgs and W bosons, respectively. A deeper understanding of the kinematics is described in the next section.

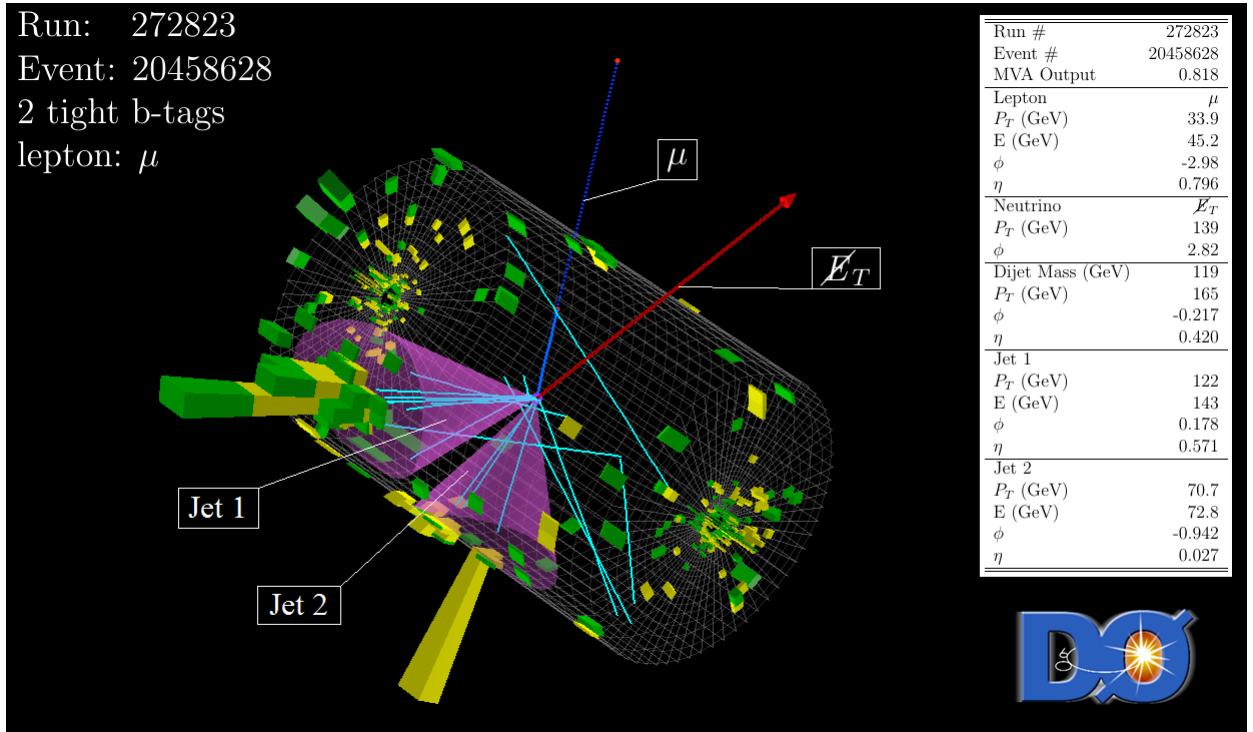


Figure 16: Event display of a likely Higgs event. The two violet cones represent the two leading jets, likely due to the decay of a Higgs boson. The muon track is a thin blue line running roughly parallel to the red missing transverse energy arrow.

The same event can be displayed in many different useful orientations, such as the side-on view of the detector (Figure 17) or the top-down orientation (Figure 18). The energy distribution of the event within the calorimeter can be seen at many different viewpoints in the multiview image (Figure 19).

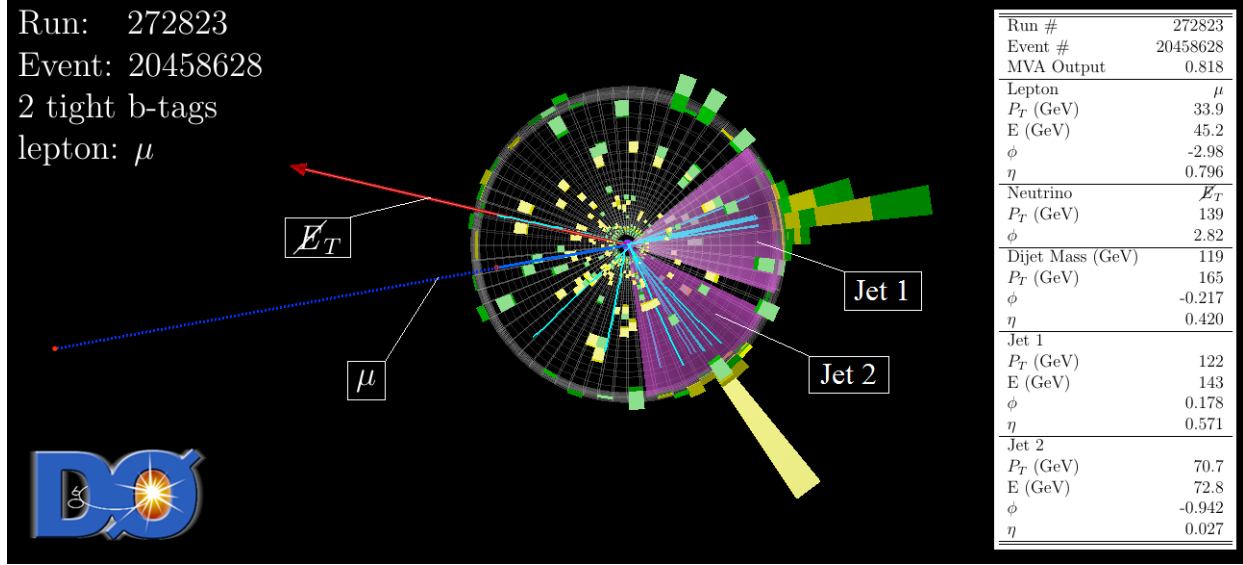


Figure 17: A side-on view of the likely Higgs event within the detector.

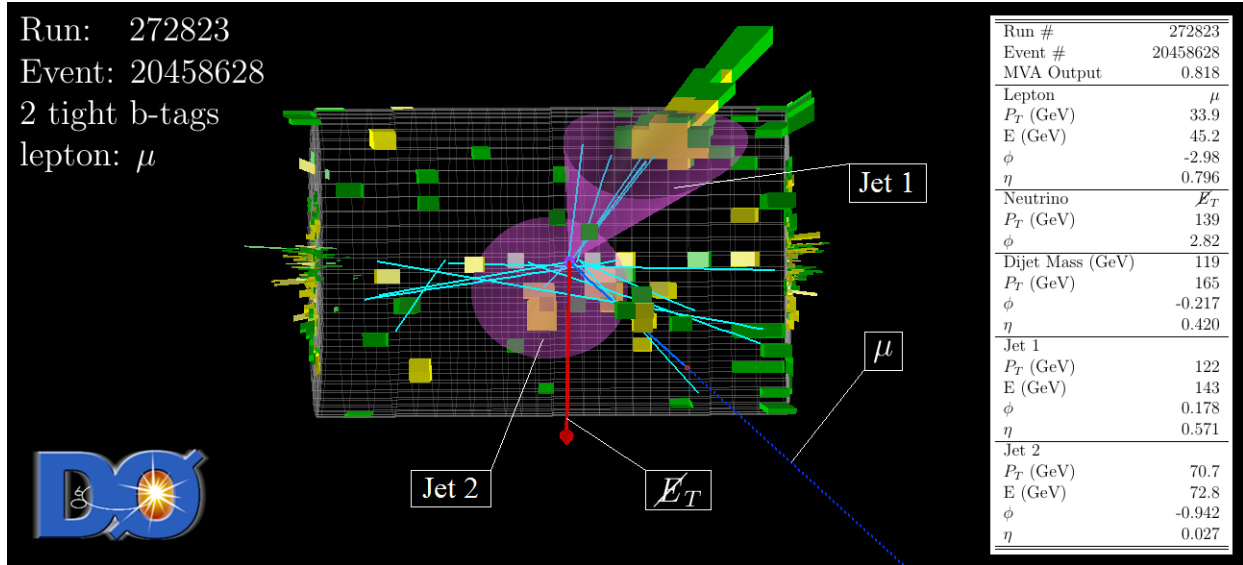


Figure 18: A top-down view of the likely Higgs event within the detector.

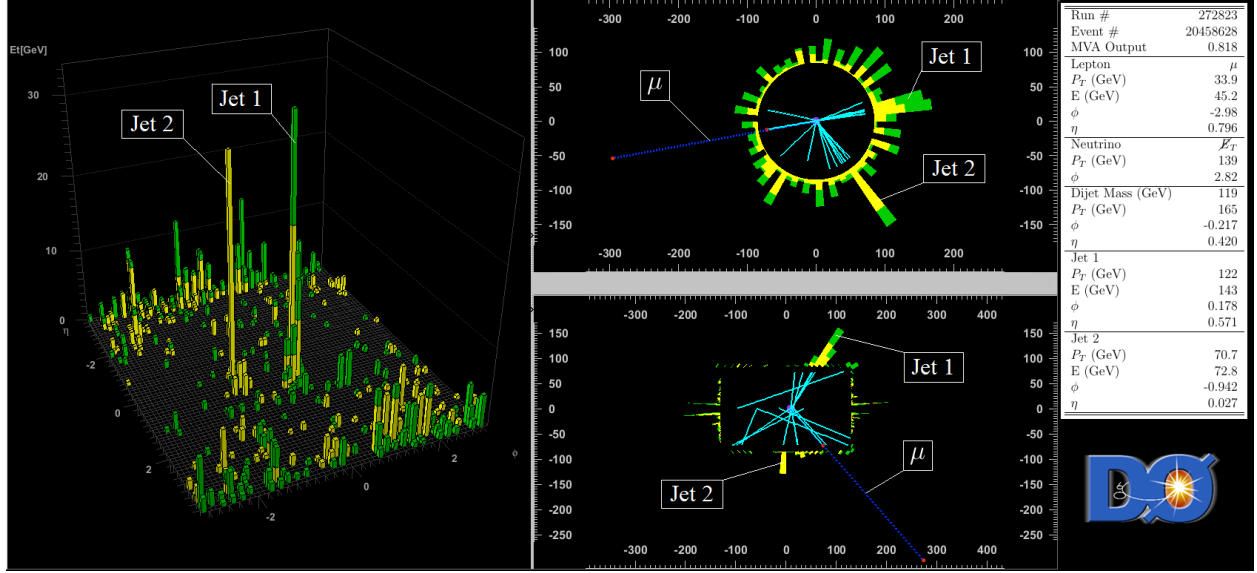


Figure 19: A multiview image of the distribution of the event's energy within the calorimeter. The energy of the two leading jets can be seen as large spikes of both electromagnetic (yellow) and hadronic (green) energy deposits, whereas the muon and neutrino deposit no energy.

4 Kinematic calculations

A. Event overview In this chapter, the properties of Higgs events as measured by DØ will be discussed through a relativistic kinematic approach. In an event, a Higgs boson is produced alongside a W boson from the quark-antiquark interaction provided by the Tevatron. The Higgs (of mass 125 GeV) most likely decays into a bottom-antibottom quark pair, which is resolved within the detector as two jets separated by a certain angle, called the dijet angle (to be discussed in detail in the next section). The $H \rightarrow b\bar{b}$ system is referred to as the dijet system. Meanwhile, the W boson decays leptonically; this system, $W \rightarrow l\nu$, is referred to as the leptonic system.

In an ideally theoretical case, the two quarks which collide at the interaction point of the collider have equal and opposite momenta in the lab frame. If this is the case, the total momentum of the system is zero, and thus any system produced immediately from the collision must also have a zero total momentum due to momentum conservation. In the case of a Higgs event, this implies that the Higgs and W bosons will have equal and opposite momenta (presumably after the decay of a virtual W boson, which won't be described in this paper). However, this does not imply a momentum distribution which is necessarily perpendicular to the beamline, as shown in the space diagram (Figure 20). In fact, in an ideal theoretical case, the equal-and-opposite momenta should be distributed randomly through any orientation in space regardless of the position of the beamline. The special perpendicular case is shown for convenience in the space diagram.

However, the momenta of the colliding quarks are not necessarily exactly equal and opposite, as assumed. The partons' (quarks and gluons, the "parts" of the proton) energies are likely distributed unequally, according to a certain parton distribution function. The

energies and momenta of the partons are constantly shifting about within the proton (and antiproton), allowing for a non-zero total momentum between the two incident quarks upon collision. This momenta distribution is very important in attempting a kinematics approach, and it must be accounted for in order to understand the event in an even approximately legitimate way. This will become apparent in the next section.

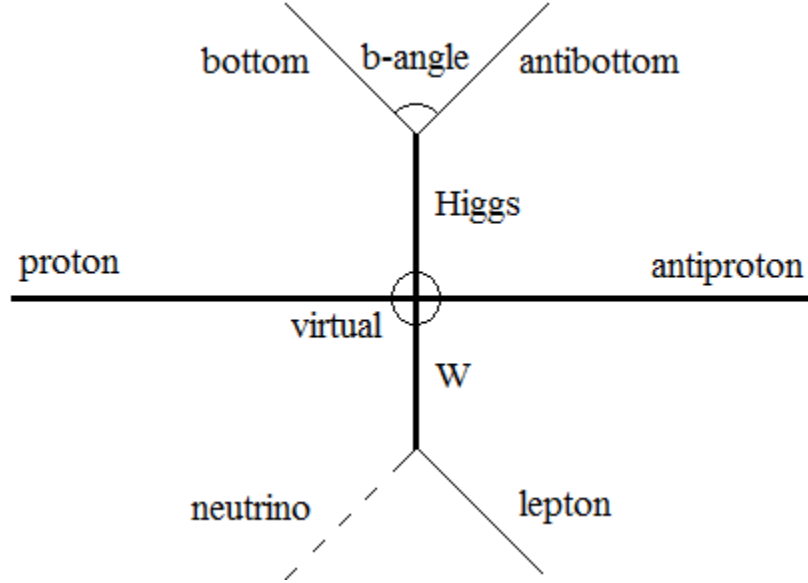


Figure 20: An idealistic space diagram of the kinematics of a Higgs event. Higgs and W boson are produced by the collision via virtual W decay (central circle). The two trajectories are back-to-back in an optimal event. The Higgs decay into a $b\bar{b}$ pair (top of diagram), while the W decays into a lepton-neutrino pair (bottom of diagram). The angle between the two bottom quark jets (dijet angle) is labeled b-angle.

Although the total momenta distribution is unpredictable within each event, the transverse momenta (perpendicular to the beamline) should always sum to about zero. Thus, parallel momenta might not be equal and opposite, but the transverse momenta of the two systems should remain roughly equal and opposite, because differences in beam energy would affect momenta only parallel, not transverse. To check for this specific equal-and-opposite nature of the systems, plots of the two systems' transverse momenta plotted against each other are shown in Figures 21 (electron) and 22 (muon). The amount of correlation implies a roughly equal-and-opposite nature for the transverse momenta between the two, as predicted.

A seemingly much more likely space diagram for a Higgs event is shown in Figure 23. In this case, the parton within the proton has a slightly greater momentum than the antiproton parton. Hence, there is a total momentum slightly to the right, and so the sum of the momenta of the two post-collision systems should be the same. The transverse momenta, however, should remain roughly equal and opposite as shown.

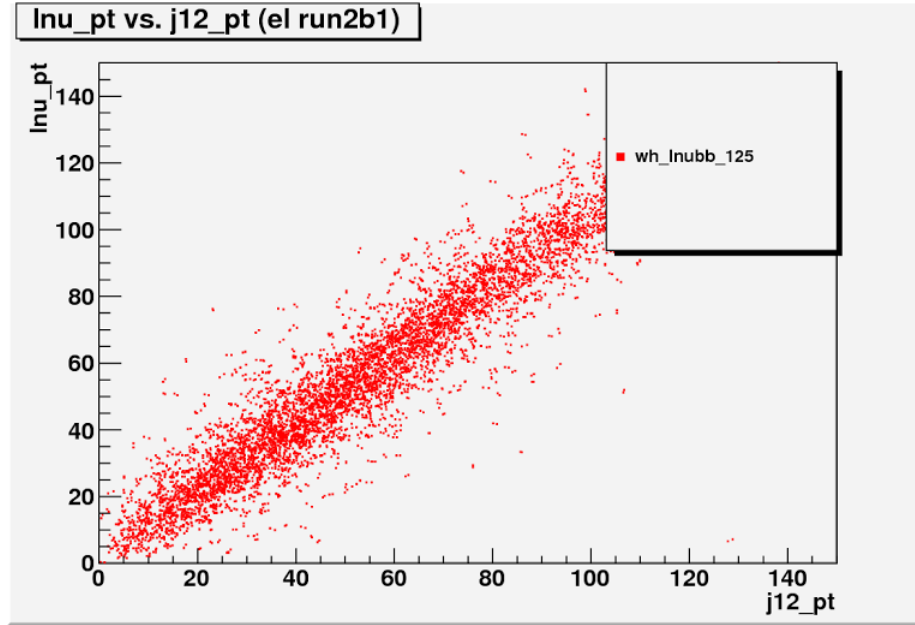


Figure 21: Correlation between transverse momenta of dijet system and lepton-neutrino system within electron events.

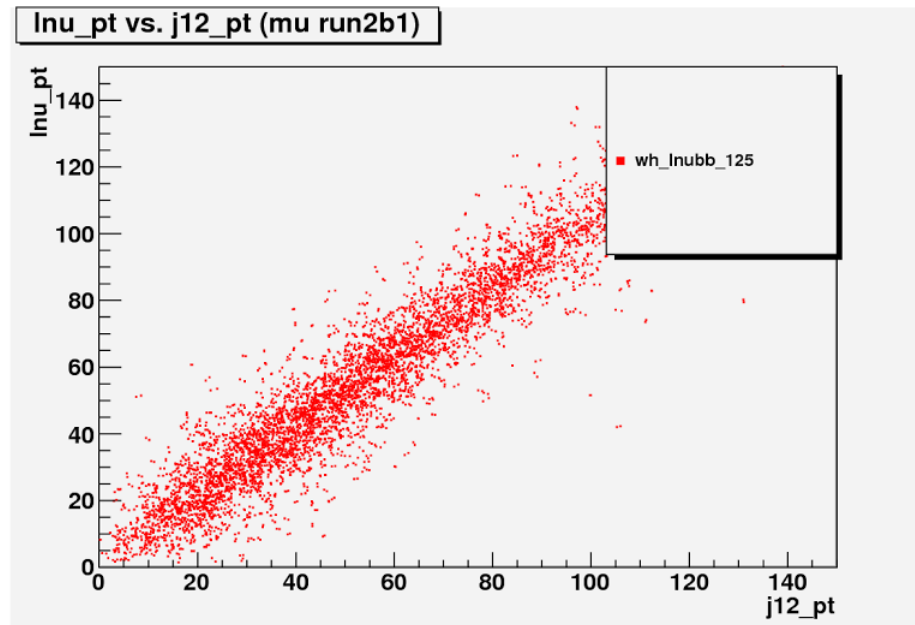


Figure 22: Correlation between transverse momenta of dijet system and lepton-neutrino system within muon events.

[These two-dimensional scatter plots courtesy of Ben Rabe of the WH $D\bar{O}$ group.]

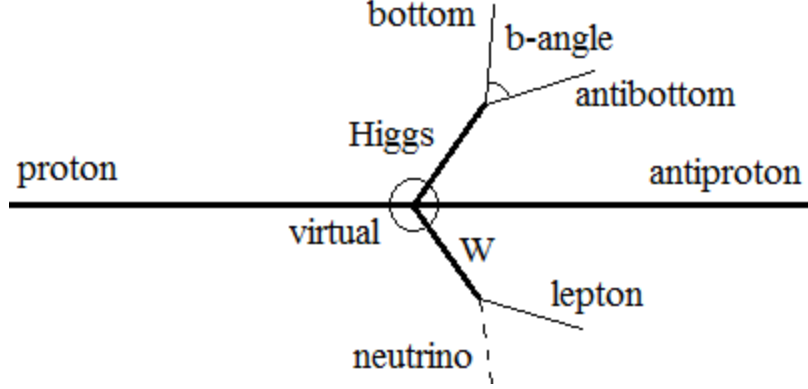


Figure 23: A space diagram showing a non-zero total momentum. In this case, the parton in the proton has slightly more energy than the parton in the antiproton, so the momenta of the two post-collision systems are not exactly back-to-back in the lab system.

B. Dijet angle calculation One of the variables of particular interest within this paper is the angle between the two partonic jets produced by the decay products of the Higgs boson. This dijet angle is directly related to the relativistic energy of the parent Higgs. The equation which is derived below, however, is simply the special symmetric case of the more general relation (which takes into account the isotropy of the decay). A more complete relativistic calculation is explained in the Appendix. The calculation of the special case is sufficient in order to illustrate the importance of energy considerations within kinematic calculations.

The Higgs decay sought in this experiment produces $b\bar{b}$ pair, each quark with an identical mass M_b of roughly 4.2 GeV, whereas the Higgs mass M_H is around 125 GeV according to the recent measurement by the LHC. The masses of the decay products are equal, and the decay in this special case is symmetric about the original parent trajectory. The parallel (to the original Higgs trajectory) momenta P_{bp} of the decay products will sum to the original momentum. Therefore, by the symmetry of this special case and conservation of momentum:

$$2P_{bp} = P_H. \quad (1)$$

Similarly, the energy E_b of each decay product is identical in this special case; their sum is the total energy, which is conserved through the decay, originally E_H . In other words, $2E_b = E_H$, or equivalently, $4E_b^2 = E_H^2$. From this energy conservation, of course, a useful relation arises for the total momenta of each bottom quark in terms of the Higgs momentum:

$$P_b^2 = \frac{1}{4}(P_H^2 + M_H^2) - M_b^2. \quad (2)$$

The relation between the dijet angle θ and the quark momentum is given simply by a trigonometric relation:

$$\cos\left(\frac{\theta}{2}\right) = \frac{P_{bp}}{P_b}. \quad (3)$$

Therefore, by substitution of Equations (1) and (2):

$$\cos\left(\frac{\theta}{2}\right) = \frac{P_H}{\sqrt{P_H^2 + M_H^2 - 4M_b^2}}. \quad (4)$$

By substituting mass values, a useful approximate relation is given for the special case:

$$\cos\left(\frac{\theta}{2}\right) = \frac{P_H}{\sqrt{P_H^2 + 15555 \text{ GeV}^2}}. \quad (5)$$

Therefore, the dijet angle is dependent completely upon the momentum of the parent particle (the Higgs), which, in turn, is dependent upon the total energy of the collision provided by the Tevatron. As stated previously, the Tevatron accelerates two beams up to about 1 TeV for each proton (or antiproton) within the beam. However, a single quark from each nucleon provides the energy in the collision, not the entire proton. Therefore, the sum of the two incident quark energies determines the dijet angle observed in the detector.

One might assume as a rough estimation that each of the nucleons' three quarks (2 up, 1 down) contains about one-third of the total nucleon energy, or roughly 330 GeV for each quark. Assuming conservation of energy within the reaction, this fixed quark energy would produce a set dijet angle of about 43 degrees. This is nothing at all like what is predicted by Monte Carlo simulations, as shown in Figure 24.

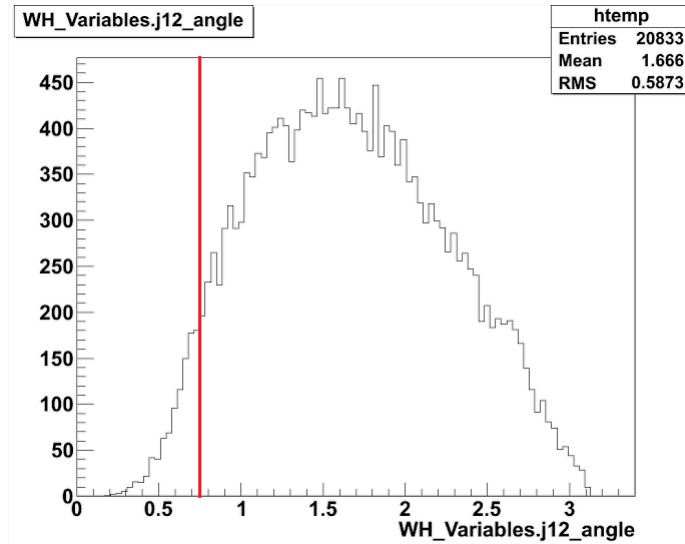


Figure 24: A histogram of Monte Carlo dijet angle data versus the predicted fixed value assuming quark energies of one-third of the nucleon energy.

C. Energy distribution considerations The previous model obviously does not agree with Monte Carlo data, and is evidence of the fact that the quark energy approximation used is quite incorrect and far too crudely generalizing. The parton model of the proton is much more complex than a simple three-quark model, but yields much more consistent results. Besides the three quarks residing within the proton, there exists a churning sea of gluons

and additional fleeting quark-antiquark pairs. All of these contribute a small fraction of the total proton energy. This distribution of energy among the parts of the proton is determined by parton distribution functions (PDFs). As one can see in Figure 25, the PDF plot shows a most probable up quark momentum fraction (x) of roughly 0.2, and similarly about 0.1 for the down quark (where each value represents $xf(x)$, the fraction of total momentum). A weighted average of these maximal values (2 up for 1 down) yields an estimated probable energy fraction of about 0.167, and therefore about 165 GeV on average for single quark energy, which is half the energy as previously assumed.

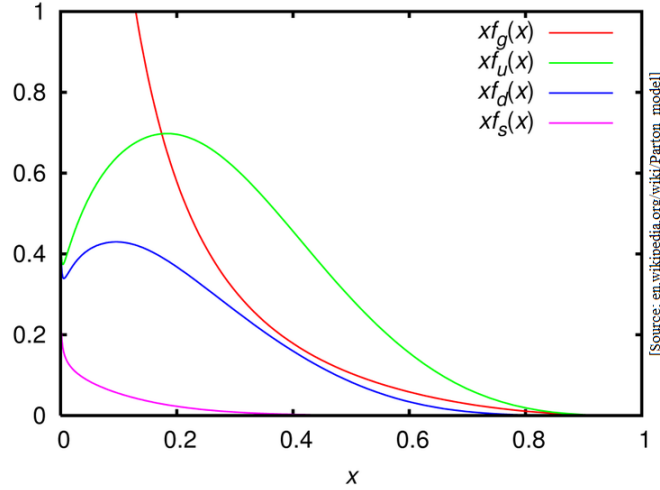


Figure 25: Parton energy distribution functions for the constituents of a proton. Plotted horizontally is the momentum fraction x for each parton. Plotted vertically is the fraction of the total momentum carried by a parton, given by $xf(x)$, where $f(x)$ is the parton distribution function.

This average quark energy yields momenta of about 128 GeV for both the Higgs and W systems, again by conservation of energy. This momentum corresponds to a dijet angle of 88.5 degrees, or 1.55 radians as shown in Figure 26. This represents the most likely value for the dijet angle, not necessarily the mean, although both are very similar in this case.

This model seems to agree very well with Monte Carlo at the most likely dijet angle, but it agrees in other ways as well. For instance, it is significant that the PDF is nonzero as x approaches zero. This explains the linear trend of the histogram at large angles (low energies). The distribution of the dijet angles is directly correlated with the integral of $xf(x)$; as x goes to zero, the area under $xf(x)$ decreases relatively linearly along with the angle distribution. Similarly, on the other end of the spectrum, the PDF approaches zero as x approaches unity. The result of this is a tailing off in the angle distribution at smaller angles (higher energies). The area under $xf(x)$ stays relatively constantly small (almost zero) as the energy fraction approaches one, and thus the angle histogram shows very small values as the dijet angle becomes smaller due to higher energies.

The exact formation of the parton distribution functions is unable to be fully formulated with QCD calculations; instead the functions are mapped through experimentation and do not currently have a known analytic form described by theory. However, the PDFs can be

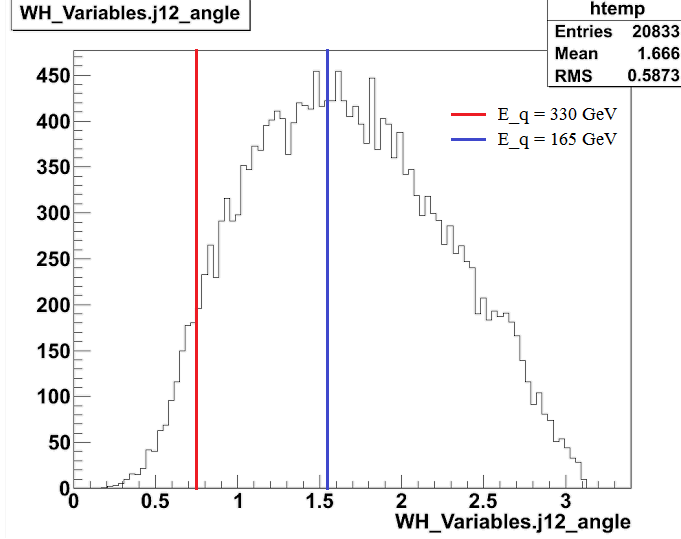


Figure 26: A histogram of Monte Carlo dijet angle data, including predicted values given both quark energies of 330 GeV (red) and 165 GeV (blue).

approximated by fitting other functions to them, such as a Gaussian for instance. Gaussian functions were fit to $xf(x)$ for up and down, which are shown in Figure 27 (left). These fits were then divided by the momentum fraction x in order to achieve the parton distribution function by itself, also shown in the Figure 27 (right). The PDF alone displays the fraction of partons that carry a certain momentum fraction, whereas $xf(x)$ displays the fraction of the total momentum that is carried by those certain partons. In order to randomly sample parton energy values from the distribution, much like a Monte Carlo simulation, the PDF itself should be used, not $xf(x)$.

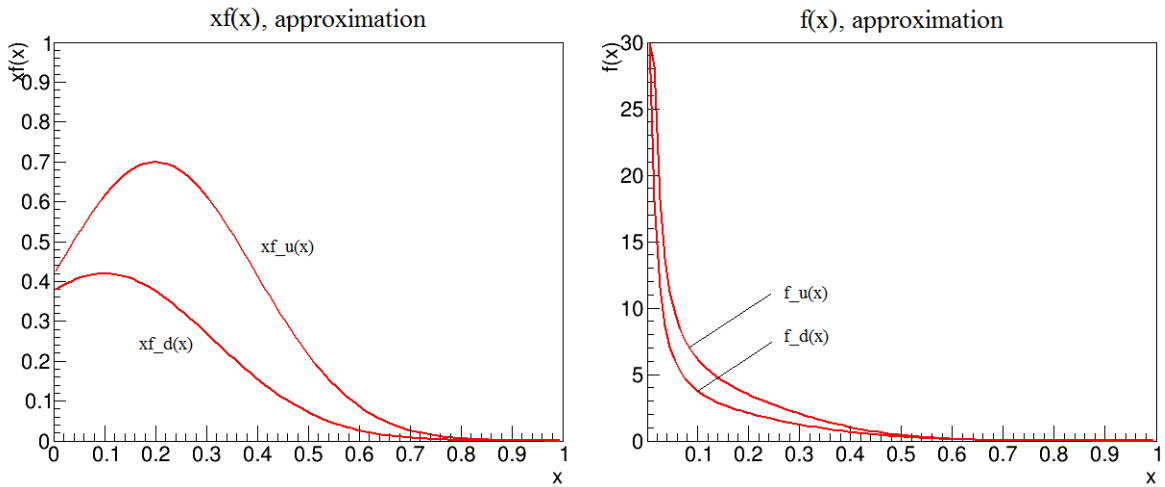


Figure 27: Plots of approximations of the product of the PDF $f(x)$ (for u and d) and the momentum fraction x versus momentum fraction (left) and isolated PDF versus x (right).

Many random energy values were chosen in this way according to the parton distribution function, which were weighted in a two-to-one fashion for the up-to-down ratio for a proton. For each simulated event, this was performed twice (once for each of the incident quarks) and were added together to achieve the total energy of the system. From this initial energy, the momentum of the Higgs system (as well as the W) is calculated according to

$$E_0 = E_H + E_W = (P^2 + M_H^2)^{1/2} + (P^2 + M_W^2)^{1/2}. \quad (6)$$

This equation assumes that the two systems have equal momenta magnitude, which is a roughly reasonable assumption, especially if the event is approximately back-to-back. The dijet angle is calculated according to its relation to the system momentum derived previously. A ROOT histogram of the dijet angle distribution for over 150 000 events is shown in Figure 28, as compared to the original Monte Carlo distribution.

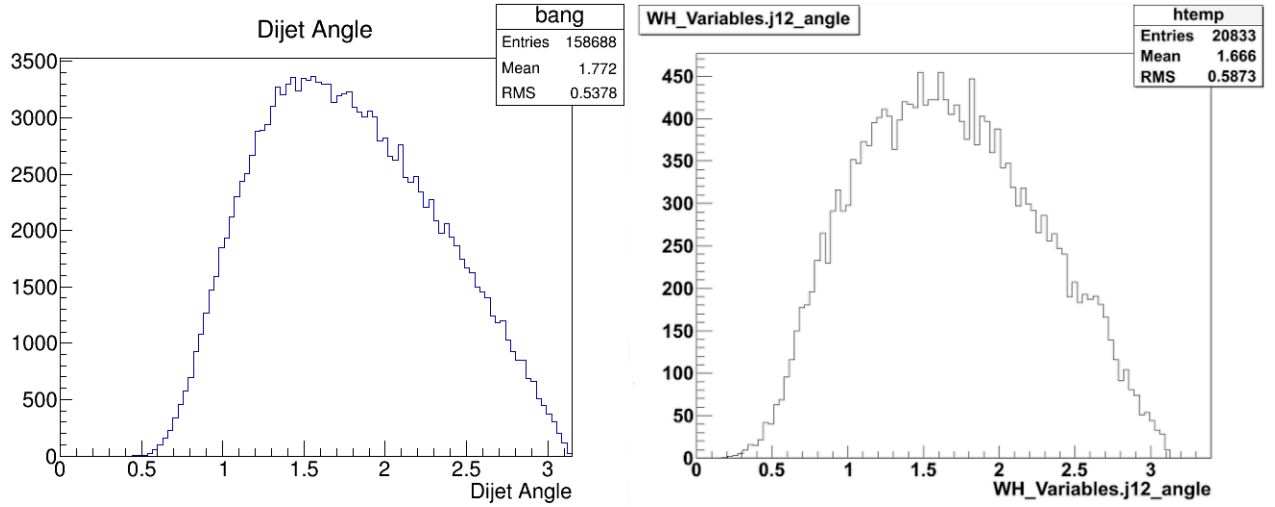


Figure 28: Comparison of simulated dijet angle distributions: At left, the distribution calculated via kinematics and approximations of parton distribution functions (the result of this section); and at right, the original Monte Carlo distribution of dijet angle among simulated Higgs events.

The histograms are very similar and follow the same general shape. One difference however, is the distribution at small angles. This high-energy deviation is possibly due to the fact that only a special case calculation was performed for the dijet angle relation to Higgs energy (see Appendix). The difference may also be the result of the equal momenta approximation for the two systems, or inexact fitting of the PDF with the Gaussian at high momenta fractions, or possibly even an inaccuracy within the original event simulation itself. All in all, however, this new distribution simulation agrees well with the original Monte Carlo simulation, generated by the $p\bar{p}$ event simulator Pythia.¹ This agreement could not have been possible without the careful consideration of parton energy distribution within the kinematic calculations of the dijet angle.

5 Conclusions

Higgs analysis has been in process for over twenty years at DØ at Fermilab, and this summer of 2014 was no exception. The WH group is continuing analysis in different forms in order to achieve significant results. The summary of work included in this paper is but a brief introduction to the work and progress made up to this summer. Additional progress, most notably the jet systematics work done by the rest of the WH group, is currently under way and near completion. Additional analytic attempts can be made in the future via a matrix element method of analysis, as was briefly discussed throughout the summer. As always, promising Higgs event displays, such as those provided in this paper, provide useful insight and visualization of the workings of particle physics of a Higgs event within the DØ detector.

Much of my summer was focused on simply attempting to learn and understand the above work done thus far within the WH group. It is a great effort and takes much time to comprehend in its entirety (which I am still attempting to do). When I was not entirely focused on this task, much of the remaining time of my summer was spent working on the kinematic calculations as described in the paper. The goal of these calculations was to understand the nature of a Higgs event within a very simplistic physical model without the complicated details of particle physics. Such a simple model is possible and is able to yield realistic results, as compared with the widely used simulations provided by high-energy event simulators such as Pythia. However, it was clearly shown that the basic understanding of the energy distribution within the parts of the proton is of utmost importance; without this parton energy distribution within the kinematics, the calculations are useless.

6 Acknowledgments

First and foremost, I would like to thank the United States Department of Energy and Fermilab for the invitation to work at such a great physics lab over this past summer. It has been an honor and a privilege. Of course, I would like to thank my mentor, Dr. Ryuji Yamada, who has been leading me and the WH DØ group throughout the summer. Also, thank you to Ben Rabe for putting up with me and my questions for these past several weeks. Thanks to the rest of the DØ group as well for putting such great work together into a single collaborative effort. Of course, thank you very much to Dr. Brad Plaster for all the help (particularly with the parton distribution functions) and support given from back home at the University of Kentucky. Finally, thank you very much to my friends and roommates Todd Seiss and Eduardo Ibarra García Padilla for the help and support all summer long.

Appendices

[Much credit to Todd Seiss for help with calculations and graphs within this appendix.]

Higgs decay Imagine a Higgs boson moving with momentum P_H in the x direction as measured by the lab frame. The Higgs then decays into a pair of b quarks. Within the Higgs' rest frame, the b trajectories are back-to-back. The angle these trajectories make with the x direction is evenly distributed (the decay is isotropic). This translates to a distribution of different opening angles when the system is Lorentz boosted into the lab frame.

The four-momentum of one of the decay b quarks in the Higgs' rest (primed) frame is

$$\vec{P}_b' = (E_b', P_b' \cos \theta', P_b' \sin \theta', 0). \quad (7)$$

Within this rest frame, $P_H' = 0$ and therefore $E_b' = \frac{1}{2}M_H$ and $P_b' = \sqrt{\frac{1}{4}M_H^2 - M_b^2}$.

The appropriate Lorentz transformation Λ in the x direction is the matrix

$$\Lambda = \begin{pmatrix} \gamma & \gamma\beta & 0 & 0 \\ \gamma\beta & \gamma & 0 & 0 \\ 0 & 0 & 1 & 0 \\ 0 & 0 & 0 & 1 \end{pmatrix} \quad (8)$$

where γ and β are the relativistic properties of the Higgs boson within the lab frame. The four-momentum of the quark in the lab (unprimed) frame is therefore given by

$$\vec{P}_b = \Lambda \vec{P}_b' = \left(\frac{1}{2}M_H\gamma + \gamma\beta P_b' \cos \theta', \frac{1}{2}M_H\gamma\beta + \gamma P_b' \cos \theta', P_b' \sin \theta', 0 \right). \quad (9)$$

The decay angle of the quark in the lab frame can then be given by the relation

$$\cos \theta = \frac{\vec{P}_{bx}}{\sqrt{\vec{P}_{bx}^2 + \vec{P}_{by}^2}} = \frac{\frac{1}{2}M_H\gamma\beta + \gamma P_b' \cos \theta'}{\sqrt{\left(\frac{1}{2}M_H\gamma\beta + \gamma P_b' \cos \theta'\right)^2 + (P_b' \sin \theta')^2}}. \quad (10)$$

This relation reduces to Equation 4 in the dijet angle calculation in the case that $\theta' = \pi/2$:

$$\cos \theta = \frac{\frac{1}{2}M_H\gamma\beta}{\sqrt{\frac{1}{4}M_H^2\gamma^2\beta^2 + P_b'^2}} = \frac{P_H}{2\sqrt{\frac{1}{4}P_H^2 + P_b'^2}} = \frac{P_H}{\sqrt{P_H^2 + M_H^2 - 4M_b^2}} \quad (11)$$

where θ in this equation is half of the opening dijet angle within Equation 4.

The relation given by Equation 10 can be equivalently expressed as

$$\tan \theta = \frac{\vec{P}_{by}}{\vec{P}_{bx}} = \frac{P_b' \sin \theta'}{\frac{1}{2}M_H\gamma\beta + \gamma P_b' \cos \theta'} = \frac{\sin \theta'}{\frac{P_H}{2P_b'} + \frac{E_H}{M_H} \cos \theta'} \quad (12)$$

The unprimed opening angle is dependent upon the primed angle and Higgs momentum.

Graphs of unprimed theta versus primed theta are shown in Figure 29 for various Higgs momenta. The straight line indicates the case where the Higgs is at rest within the lab frame and so all decays are back-to-back. Greater Higgs momenta correspond to more greatly bent curves.

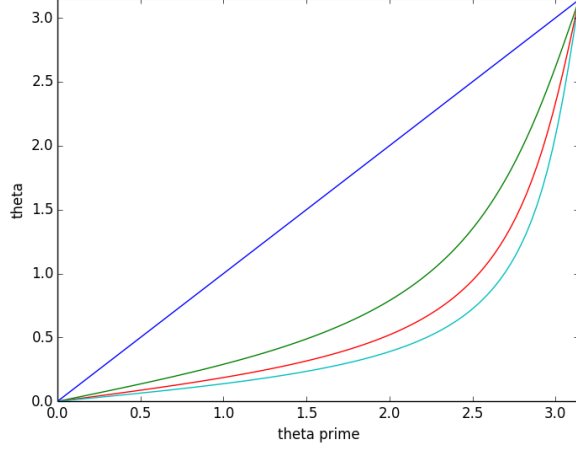


Figure 29: A graph of unprimed angles versus primed angles at various Higgs momenta.

The average value of these angle distributions can be calculated numerically at various momentum values. A plot of the average angle versus Higgs energy is shown (in blue) in Figure 30. Also shown in the graph is the original dijet angle relation to energy (in green), as derived from Equation 4. It is clear that the approximate angle relation underestimates the true distribution, especially at greater Higgs energies. The relations become equivalent at the classical limit when the Higgs energy approaches its rest mass.

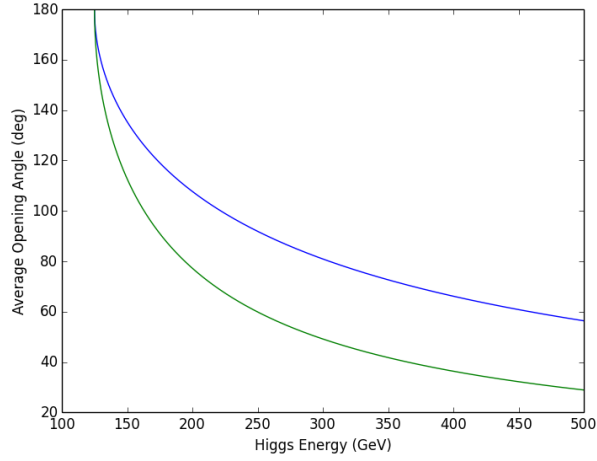


Figure 30: A plot of the average angle versus Higgs momentum (blue). Also shown is the original approximation (green). The approximate relation underestimates the average angle.

These two relations display the same important inverse relationship between the opening angle and momentum. In this regard, it may serve as an adequate approximation when one calculates over a large distribution of momenta. As concluded within this paper, the energy distribution is of even greater importance than the isotropy of the decay to the distribution of angles. Even so, the underestimate of the angle histogram at large energies as compared to original Monte Carlo is likely due to the approximate nature of the kinematic calculations.

References

- [1] The DØ Collaboration. Updated search for Higgs boson production in final states with a lepton, missing energy, and at least two jets in 9.7 fb^{-1} of Tevatron data. DØ Note 6346-CONF, July 2012.
- [2] Savanna Marie Shaw. *Search for the Standard Model Higgs Boson in Association with a W Boson at D0*. PhD thesis, Michigan State University, 2013.